19th Brazilian Congress of Thermal Sciences and Engineering
November 6th–10th, 2022, Bento Gonçalves - RS - Brazil

# ENC-2022-0593
# Numerical Study of Triple Flames in Partially Premixed Methane and Hydrogen-Air Mixtures

**Rafael Becker Meier**[a]
**Thiago Cardoso De Souza**[b]
**Amir Antônio Martins Oliveira**[a]
Federal University of Santa Catarina, Brazil[a]
Federal University of Rio Grande do Norte, Brazil[b]
rafael.meier@labcet.ufsc.br

***Abstract.*** *The local burning rate and the associated structural variations of laminar triple flames are investigated using direct numerical simulations (*DNS*) with detailed chemical reaction mechanisms for two distinct fuel-air mixtures,* $CH_4-$*air and the* $H_2-$*air mixtures. The simulations were performed through a parametric variation based on the mixing layer thickness. The triple flames are initiated by imposing a heat source in the center of a scalar mixing layer of non-uniform thickness. The results show that the methane flame propagation is ruled by the flow that develops at the local stoichiometric condition associated with the triple point. On the other hand, the hydrogen leading edge is dominated by the richer region where the burning rate is higher. The mixing layer thickness causes an impact on the magnitude of the flame deformation where for smaller profile thicknesses the lean flame stabilizes even in the flammability limit conditions. Consequently, the local stretch rate and the displacement speed undergo substantial variations where the front curvature increases for decreasing values of the mixing length. The correlation between the local flame speed and the Karlovitz number,* $Ka$*, shows that the expected behavior, related to the Markstein length,* $Ma$*, is not required in a partially premixed flame according to the premixed properties.*

***Keywords:*** *triple flames, direct numerical simulations (*$DNS$*), stretch rate, burning rate*

## 1. INTRODUCTION

Triple flames, also referred as tribrachial or edge flames, are flame configurations specially relevant for the analysis of partially premixed combustion. In partially premixed combustion, although the fuel-air mixture is mixed up to a certain degree, the mixture is not fully mixed in its entirety before the establishment of the combustion process. A series of investigations, Im and Chen (2001), have shown that the combustion analysis of triple flames provides a significant understanding of the stabilization mechanism associated with turbulent diffusion flames, giving valuable insights into the phenomenon of flame spreading and autoignition of flame structures related to the partial premixed regime.

The investigation of the stabilization mechanism of lifted flames is a relevant topic in turbulent combustion. For example, in the case of triple flames, the stabilization point, referred as the triple point, involves a complex interaction of the incoming partial premixing of reactants with local unsteady aerodynamic effects, such as the strain rate promoted by the presence of turbulent eddies at the flame front. In fact, as pointed out by Im and Chen (1999), the knowledge of the dynamics of these flames is required when one considers the appropriate design and development of practical devices operating with partially premixed combustion. In technical applications, the optimum performance often lies somewhere between the extremes of premixed and non-premixed combustion, trying to profit from advantageous features of both while avoiding their adverse effects in a stratified medium, Peters (2001). The partially premixed flames can be found in direct injection gasoline engines, aircraft gas turbines, diesel engines and in lift-off and stabilization of turbulent jet diffusion flames, specifically, in industrial burners and flaring operations, See and Ihme (2015); Benajes *et al.* (2013); Cadrazco *et al.* (2020); Mosiria *et al.* (2018).

In this paper, triple flames associated with two distinct fuel-air mixtures are investigated, methane $CH_4-$air and the hydrogen $H_2-$air mixtures. Considering the latter case, in fact, hydrogen or hydrogen enriched fuels are currently treated as an promising strategy to reach sustainable clean combustion, its implementation as fuel provides a viable solution to the increasing demand of clean and secure energy, Masri (2021). However, the transition from fossil fuels to such new burning technologies involves many challenges that must be overcome for its widespread public use and acceptance, Ishaq

*et al.* (2022).

As an example of such challenges, when one compares with common hydrocarbon mixtures, hydrogen-air mixtures have strong preferential differential effects, and in case of triple flames the diffusion of hydrogen is amplified by the curvature of the flame tip, thereby contributing substantially to the intensification of the flame speed through chemical effects. Several differences in the flame structures also develops, for instance, while the triple point in methane triple flames is displaced towards the lean side of the mixture, in hydrogen, the triple point is located in the rich side. The high diffusivity of hydrogen, which is especially enhanced in the region of high flame curvature, may affect significantly the local propagation of the flame front, Im and Chen (2001).

This paper is within the scope of a broader investigation that considers the effects of spatial and temporal modulation of partially premixed flames in terms of selected flow scales. Here the focus is on the aerodynamic interaction related to the flow and chemistry and the effects associated with the curvature and stability of partially premixed flames as represented by triple flames.

## 2. THEORY

Triple flames have a flame structure associated with partially premixed flames, these flames are characterized by a complex arrangement defined in terms of a certain range of mixture fractions $Z_{min} < Z < Z_{max}$, with the stoichiometric mixture fraction $Z_{st}$ lying within these limits. The leading edge of the flame is the triple point. Triple flames are always curved at the triple point. The curving process occurs due to the local burning velocity, by which the premixed branches of the triple flame propagate in the direction normal to the premixed front with an intensity that depends on the local mixture fraction. The burning velocity decreases as one moves from the triple point downstream the lean or the rich premixed branches. In these flames, the triple point propagates fastest while the rich and lean premixed flame branches stay behind, Peters (2001).

The effects of curvature and strain rate on the flame propagation speed $S_l$ are considered in terms of the following expression,

$$S_l = S_l^0 - S_l^0 \mathscr{L}\kappa - \mathscr{L}S, \tag{1}$$

where $S_l^0$ is the propagation speed of an unstretched laminar flame, $\mathscr{L}$ is the Markstein length. For example, larger values of $\mathscr{L}$ corresponds to a greater effect of curvature on the local burning velocity, the curvature $\kappa$ is given by,

$$\kappa = \frac{\partial n_i}{\partial x_i}, \tag{2}$$

and the strain rate $S$ by,

$$S = -n_i \frac{\partial u_i}{\partial x_j} n_j. \tag{3}$$

The Markstein number, $Ma = \mathscr{L}/\delta_L^0$, where $\delta_L^0$ is a characteristic length associated with the laminar flame thickness, is a dimensionless number that enables the proper quantification of the effects associated with any alteration in the flame surface topology, e.g., local flame front curvature, on the local heat release.

As will be discussed, the propagation speed of the triple flame is strongly dependent on various parameters such as the Lewis number, and the mixture fraction gradient, Buckmaster and Matalon (1989); Lee and Chung (1997); Hartley and Dold (1991); Kioni *et al.* (1993). Through the evaluation of the flow and the species field, this paper aims to investigate the effects of several parameters on the local burning velocity for different types of fuel-air mixtures. Here, the parametric analysis is formulated in terms of the evaluation of the flame strain rate, $S$, the curvature, $\kappa$, and the mixing layer thickness, $\delta_m$.

## 3. MATERIALS AND METHODS

### 3.1 Computational Methods

Direct numerical simulations (DNS) were carried out to investigate the local burning rate and the structural variations of laminar triple flames with detailed chemical reaction mechanisms for mixtures of air-methane and air-hydrogen. The compressible Navier-Stokes equations are solved using OpenFOAM (OpenCFD (2011)) as the CFD solver, with its standard capabilities coupled to the EBI-DNS (Engler-Bunte-Institute) implementation (Zirwes *et al.* (2020)), which address the detailed transport coefficients of the governing equations, i.e., the momentum, species, and energy transport equations. For methane-air simulations, the reduced mechanism of Kee *et al.* (1985) with 17 species, and 58 elementary reactions was used. While for the hydrogen-air mixture, the computations employed the Li *et al.* (2004) reaction mechanism containing

9 species and 38 elementary reactions. In order to increase the time and spatial discretization accuracy, the backward difference method together with a cubic spatial interpolation scheme were respectively used. To ensure the stability of the numerical solution, the CFL condition was set to $< 0.2$ for all simulations. In all cases a low Mach approach is used, such that the pressure-implicit split-operator (PISO) algorithm has been used for the pressure correction (Ferziger and Peric, 2002). The computational domain uses rectangular structured mesh elements with a resolution of at least 20 cells to resolve the flame thickness. In addition, a set of simulations were performed using Cantera (Goodwin (2002)) to analyze and compare the transport properties of canonical flat flames and the strain rate effect for both fuel-air mixtures.

Closely following Peters and Williams (1987), in this investigation the stretch-chemistry interaction developing at the flame front is studied considering the definition of the flame surface as the the spatial region dominated by the highest values of the high energy Arrhenius terms. Therefore, as presented in Davis *et al.* (2002), this region is the locus of maximum consumption rate of oxygen, i.e., it accurately describes the region where the fuel concentration approaches zero, and furthermore it also coincides with the region just following the radical consumption zone.

### 3.2 Configuration

The computational configuration is a two-dimensional slab subject to a prescribed inlet velocity, shown in Fig. 1, while at the sides of the domain, symmetric boundary conditions were imposed. The domain is varied depending on the case selected, in some cases it has a constant length of $L = 20$ mm and a width of $W = 5$ mm, while in other cases a length of $L = 20$ mm and a width of $W = 10$ mm. To avoid reflections of pressure waves at the inlet and at the outlet region, non-reflective boundary conditions (NRBC) are used. The flames were analysed at atmospheric pressure with an inlet temperature of $T_u = 300$ K. A composition profile of the unburned mixture based on the mixture fraction $Z$ is prescribed at the domain entrance following the procedure described in Favier *et al.* (1998); van Oijen and de Goey (2004),

$$Z_{inlet} = \frac{1}{2}(Z_1 + Z_2) + \frac{1}{2}(Z_1 - Z_2)cos\left(\frac{\pi}{2}\left(1 - \left(\frac{\pi y}{W}\right)\right)\right), \tag{4}$$

where $Z_1$ and $Z_2$ represent the lean and rich extremes of the mixture fraction, Tab. 1. For methane, $Z_1$ and $Z_2$ reproduce the flammability limits, and the stoichiometric value lies at the center of the profile. For hydrogen, due to its stretched flammability limit, Fig. 2, the variable $Z_1$ is in the lean limit of $\phi = 0.3$, whereas $Z_2$ was limited to $\phi = 4.0$. At the center of the profile, $Z = 0.056$, which corresponds to an equivalence fuel-air ratio of $\phi = 2.0$. In Tab. 1 is shown the inlet velocity, $u_{inlet} = S_l^0$, and the flame characteristic time, $\tau_f = \delta_l^0/S_l^0$, based on the stoichiometric flat flame.

One of the parameters analyzed in this study is the effect of mixture fraction thickness given by,

$$\delta_{mix}(x) = (Z_1 + Z_2)\left(\frac{dZ}{dy}|_{y=W/2}\right)^{-1}. \tag{5}$$

At the inlet, $\delta_{mix}$ is defined by $\delta_{mix}(0) = 4W/\pi^2$. For each fuel, two different cases are setup representing domains with widths of $W = 5$ and $W = 10$ mm, which are labeled as $\mathrm{W5CH_4}$, $\mathrm{W10CH_4}$, $\mathrm{W5H_2}$ and $\mathrm{W10H_2}$.

Table 1: Physical and numerical parameters.

| fuel | $\phi$ | $Z_1 - Z_2$ | $u_{inlet}$, cm/s | $\tau_f$, ms |
|---|---|---|---|---|
| $CH_4$ | 0.6 - 1.4 | 0.03 - 0.08 | 37.1 | 1.22 |
| $H_2$ | 0.3 - 4.0 | 0.009 - 0.105 | 132.0 | 0.15 |

The simulations were initially performed with pure air while the reactive mixture entered until it fills the whole domain. Then, the flames are subsequently initialized using a local patch field defined as a hot spot temperature location, such initialization is prescribed in terms of a Gaussian function of the form, (Im and Chen, 1999),

$$T(x, y) = T_0 + (T_{max} - T_0) \cdot exp[-\{x - x_c\}/\delta_{ig}^2]exp[-\{y - y_c\}/\delta_{ig}^2]. \tag{6}$$

The ignition is imposed at the center of the mixing layer at $x_c = 0.7L$ and $y_c = 0.5W$. In this study, $T = 300$ K and $T_{max} = 3000$ K, while the width of the initial temperature profile, $\delta_{ig}$, is set to have a small value of $\delta_{ig} = 0.075W$.

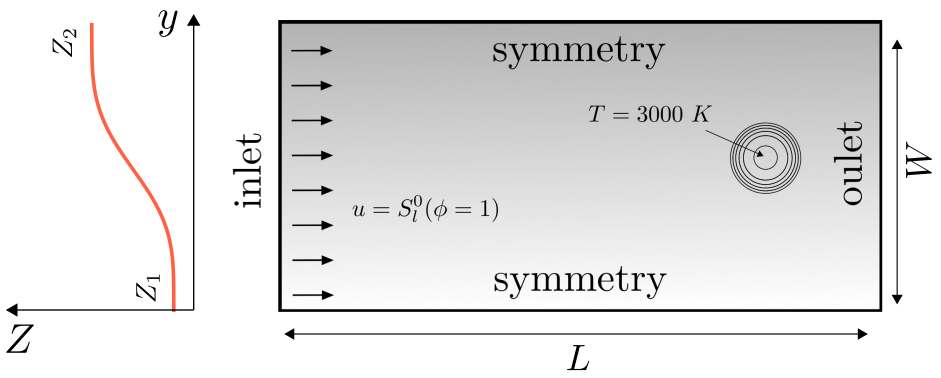


Figure 1: Initial conditions and boundary conditions for the triple flame modelling.

## 4. RESULTS AND DISCUSSIONS

Hydrogen has drastically different properties from traditional hydrocarbons, such as methane. Figure 2 compares the reference flame speed, the Markstein number, and the flame structure for both fuels. The Markstein number computations were performed closely following Davis *et al.* (2002), which uses the counter-flow model from the chemical kinetics solver Cantera. Figure 2a exemplifies two fundamental properties, namely the high flame speed and the wide flammability range related to hydrogen flames. As can be observed, even under lean conditions, the hydrogen flame shows a substantially higher speed than the methane flame under stoichiometric condition. At stretched conditions, the flames have a similar behavior from $\phi = 0.7$ up to $\phi = 1.4$, where the Markstein number, Ma, tends to decrease the flame speed. However, for equivalence ratios below 0.7, the stretch effect increases the hydrogen propagating speed since it is subject to the thermo-diffusivity instabilities associated with preferential diffusion.

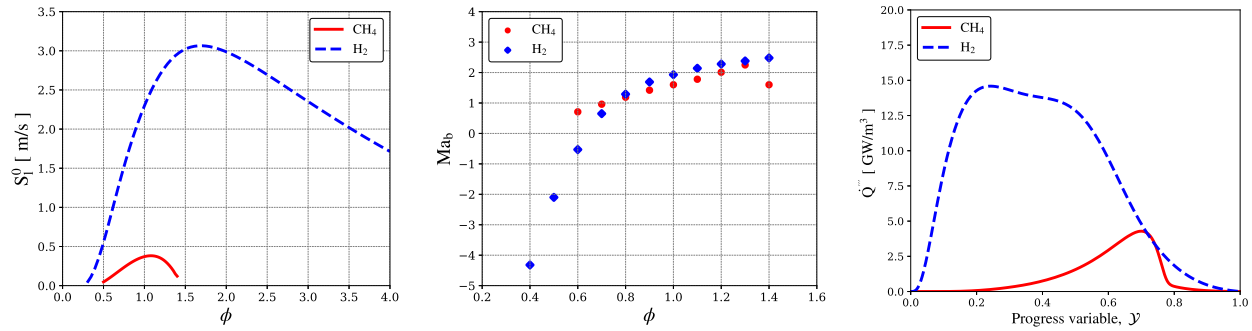


(a) (b) (c)

Figure 2: Flame propagation properties of methane and hydrogen, (a) reference flame speed, (b) Markstein number and (c) flames structure for $\phi = 1$.

According to the asymptotic flame theory, a flame is divided into a preheating zone, with a characteristic length scale $\delta_l$, and a thin reaction zone $\delta_r$, in general $\delta_r << \delta_l$. In this theory, the reaction zone is located near the burnt side of the flame structure where all reactions occur. When comparing $H_2$ and $CH_4$, the difference becomes evident in terms of a scaled progress variable, $\mathcal{Y} = (T - T_u)/(T_{ad} - T_u)$, as shown in Fig. 2c. The methane flame follows the basic asymptotic idea, that is a peak of heat release rate occurring towards $\mathcal{Y} = 1$ and $\delta_r << \delta_l$ while the hydrogen HRR peak is close to $\mathcal{Y} = 0.2$ and $\delta_r$ is not "thin" within the progress variable range. This characteristic, in addition to preferential diffusion effects, generates the distinct behavior observed $H_2$ flames when compared to hydrocarbons flames.

Figure 3 presents the contours for the $W5H_2$ (left column) and the $W5CH_4$ (right column) cases at $t/\tau_f = 16$ and $t/\tau_f = 32$, respectively. The first row of Fig. 3, shows the global framework represented by the normalized HRR regarding the stoichiometric condition, $\Omega$. The flames are not symmetric. For instance, Fig. 3a shows that for the lean region at the lower domain edge, the $H_2$ flame is continuously stretched, and the burning rate decreases until extinction occurs due to the low $\phi$. At half of the domain, the term $\Omega$ reaches the highest values since this region is composed of higher flame speeds with equivalences ratios around 1.6. From the middle to the upper domain edge, the rich side is dominated by the strain rate until the border, where a negatively curved region is formed. Figure 3b presents a different scenario for the $CH_4$ case in the leaner region. Instead of flame extinction, a negatively curved area is also developed as it occurs on the richer side.

Figures 3c and 3d show that the hydroxide radical OH is formed at regions with equivalence ratios near the stoichiometric condition where the temperature is sufficiently high, giving rise to a transport channel between the lean and rich fluxes. Figures 3e and 3f point out specific features of each fuel. In the hydrogen triple flame, the O radical is formed in the lean side, mainly at $\phi = 1$, which is not entirely consumed, being transported downstream of the flow. Figure 3f shows the presence of the methyl radical, $CH_3$, which is the first radical formed during methane combustion. It presents a higher concentration at richer conditions where the burning rate is slower, and decreases as the front becomes leaner until it vanishes.

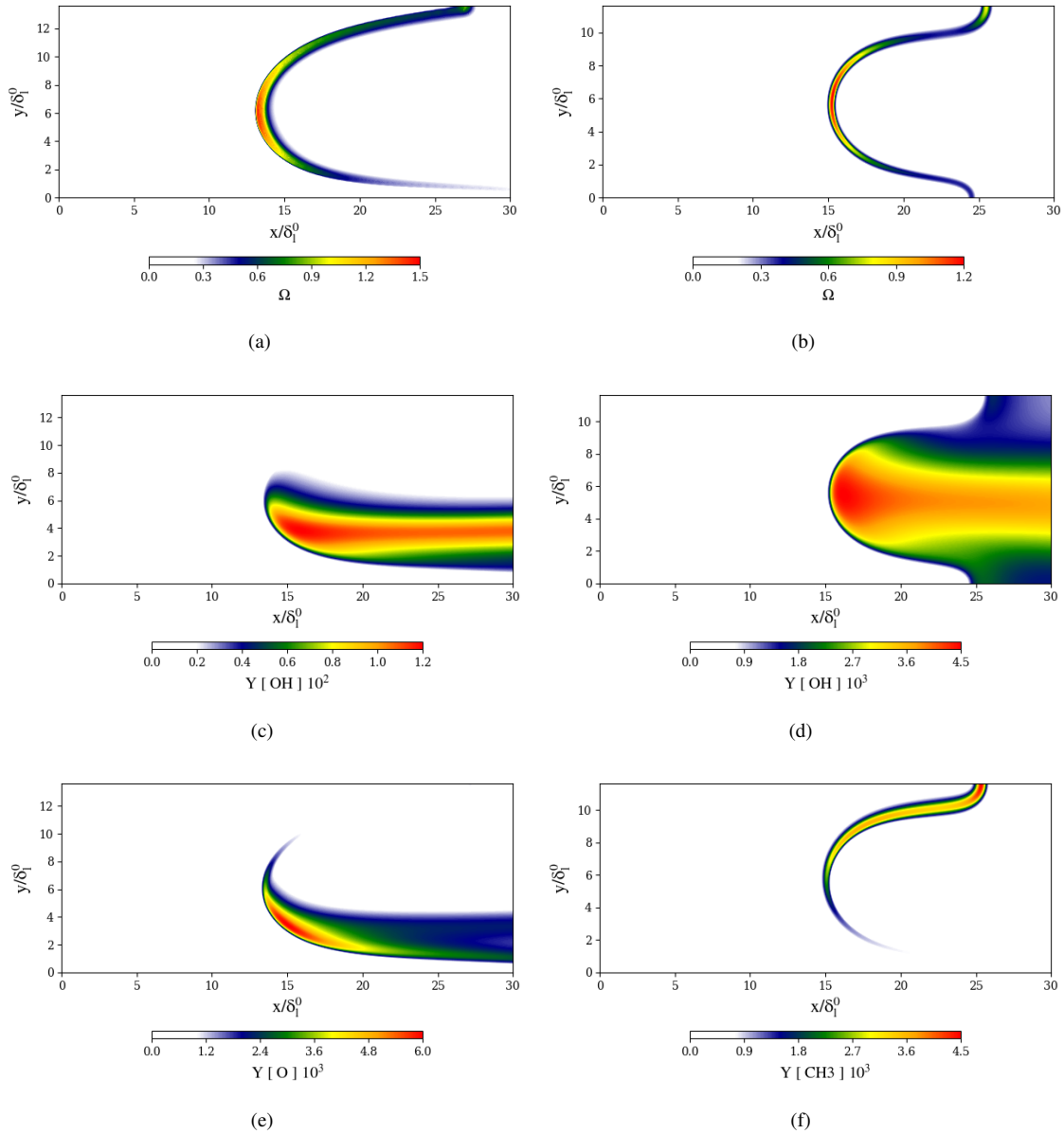


Figure 3: Partially premixed flame front for $W5H_2$ (left column) and $W5CH_4$ (right column) cases at $t/\tau_f = 16$ and $t/\tau_f = 32$, respectively. (a) normalized HRR, (c) OH mass fraction, (e) O mass fraction for hydrogen flame and (b) normalized HRR, (d) OH mass fraction, (f) $CH_3$ mass fraction for methane flame.

The flame speed and the geometry inherit the properties previously discussed. Figure 4 shows the flame weighted displacement speed, $\tilde{S}_d = \rho S_d/\rho_u$, along the normalized flame front length, $s/s_{max}$, for both four cases. Even with different propagation properties, the triple flames present common behaviors as can be seen in Fig. 4, for example the absolute speed, $S_a$, reaches higher values at the extremes locations of the domain, decreases at intermediates regions, and increases near the stoichiometric region. The flow velocity and the deformation also follows the same behavior, $S_d = -(S_a - \vec{V} \cdot \vec{n})$. Since at the domain edges, the flow deformation is much more intense than the local absolute speed, it causes an apparent increase in the local flame speed relatively to regions near the stoichiometric conditions.

Figure 4b shows the effect of the variation of the mixing layer thickness for methane flames. Around $s/s_{max} \sim 0.5$, in both cases, the flames reach the maximum absolute speed and the burning rate. The mixing layer effect apparently

generates higher values of the global flame speed for the $\mathrm{W5CH_4}$ case as a function of the normalized flame length. The thicker $\delta_m$ generates relatively high global burning rate since the flame leading edge is composed of a broader region of equivalence ratios thereby resulting in higher values of $S_l$, as shown in Figs. 4d and 4f. For hydrogen flames, Fig. 4a, the $\mathrm{W5H_2}$ case shows a similar behavior as observed in the $\mathrm{W5CH_4}$ flame. On the other hand, the thicker mixing layer in $\mathrm{W10H_2}$ causes a high strain rate, resulting in a progressive decay in the displacement speed on the lean side of the domain.

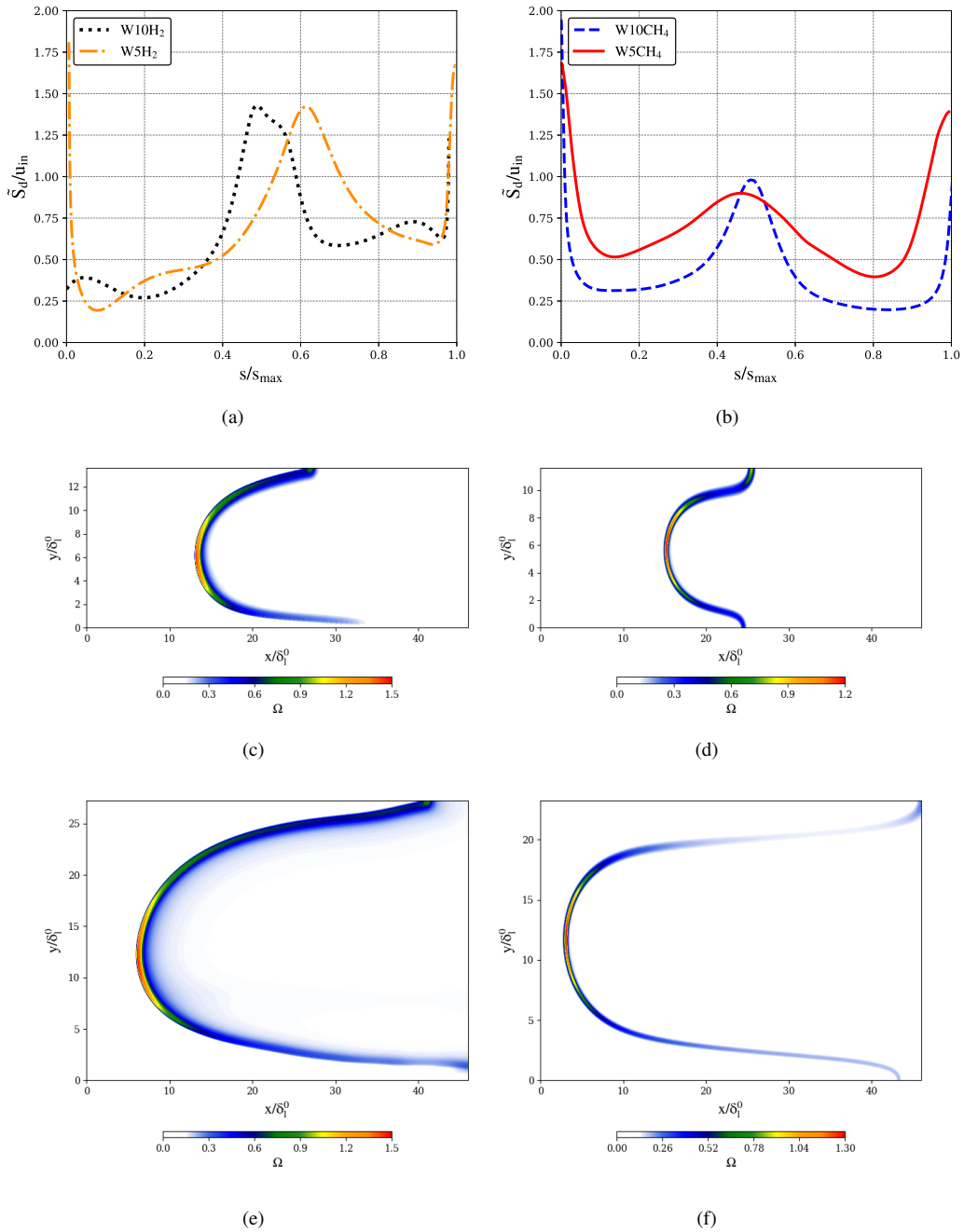


Figure 4: Normalized displacement speed and HRR for hydrogen (left column) and methane (right column) cases at $t/\tau_f = 16$ and $t/\tau_f = 32$, respectively. (a) hydrogen displacement speed and (b) methane displacement speed as function of $s/s_{max}$, and normalized HRR for (c) $\mathrm{W5H_2}$, (d) $\mathrm{W5CH_4}$, (e) $\mathrm{W10H_2}$ and (f) $\mathrm{W10CH_4}$.

Figure 5 presents the local Karlovitz number, $\mathrm{Ka} = \mathrm{Ka_s} + \mathrm{Ka_c}$, where the tangential strain and curvature effects are

$$\mathrm{Ka_s} = \frac{\delta_l^0}{S_l^0} S, \qquad \mathrm{Ka_c} = \frac{\delta_l^0}{S_l^0} S_d \, \kappa. \tag{7}$$

For all cases, the Karlovitz number was taken from the lean side to half of the domain. Figure 5a shows the curvature and the strain rate contribution to the total $\mathrm{Ka}$ for the $\mathrm{W5CH_4}$ case. In the leaner region, the negative curvature dominates

the global Ka, progressively decreasing as the equivalence ratio becomes richer, and decaying from $s/s_{max} = 0.1$ up to $s/s_{max} = 0.3$. Near the stoichiometric condition, the flame topology is made up of positive Ka due to the curvature of the flame front. Figure 5b presents the comparison between the four cases. For the cases with smaller $\delta_m$, the Ka number reaches higher values near the leading edge for both $H_2$ and $CH_4$ flames. The increasing in $\delta_m$ produces a front which is more extended and where prevails values of $Ka_c \approx 0$ in the intermediate region between $Ka < 0$ and $Ka > 0$.

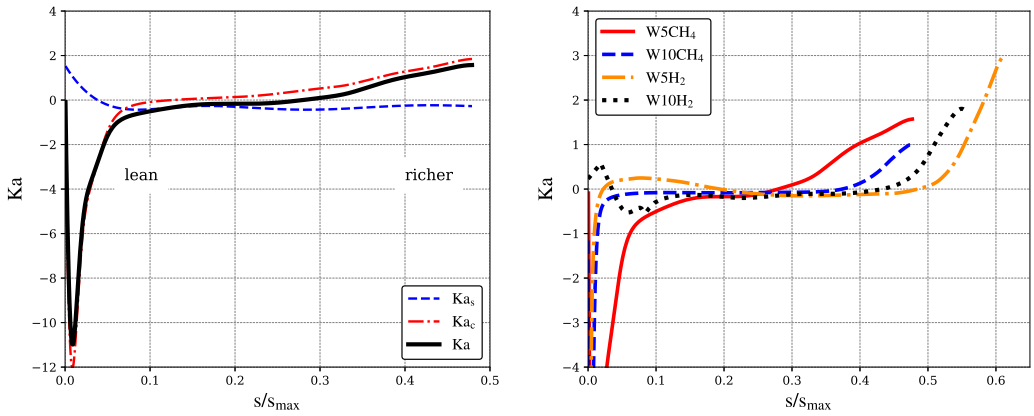


(a) (b)

Figure 5: Local Karlovitz number along the normalized flame length, $s/s_{max}$, for hydrogen and methane cases at $t/\tau_f = 16$ and $t/\tau_f = 32$, respectively, (a) total Ka and the contribution of strain rate, $K_s$, and the curvature $K_c$ in $W5CH_4$ and (b) Ka number comparison between the four cases.

Figure 6 addresses the flow-chemistry interaction through the correlation between the local flame speed and the Karlovitz number. The expected behavior, related to the Markstein length, is not imperative in a partially premixed flame according to the premixed properties. Figure 6a shows that the positively curved flame edge, where $Ka > 0$, decreases the flame speed as the stretch rate approaches zero. It corresponds to the opposite effect regarding the $Ma > 0$, observed in Fig. 2b. However, when $Ka \approx 0$, the correlations undergo an inflection where the flame speed increases as Ka decreases towards the direction of high negative values. It occurs in the leaner region, where the curvature is negative. Along the curve, the correlation undergoes another inflection towards $Ka = 0$, where the flame speed remains almost at constant values. For the cases $W5CH_4$ and $W10CH_4$, the curves present the same behavior with the effect of changes in the profile thickness, $\delta_m$, resulting in greater $\tilde{S}_d$ and Ka amplitudes in the $W10CH_4$ case in comparison to the $W5CH_4$ case. The characteristics observed in hydrogen flames are similar to methane flames but with specific features, as shown in Fig. 6b. When the normalized quantity $\tilde{S}_d/u_{in}$ approaches unity and the Ka number approaches zero, the flame speed decreases, from $\tilde{S}_d/u_{in} = 1$ up to the value of 0.25, with nearly constant values of Ka. For the $W5H_2$ case, the flow provides a negative curvature caused mainly by the variation of the profile thickness, which tends to increase $S_l$, while the flame front of the $W10H_2$ case is stretched until the domain outlet, decreasing $\tilde{S}_d$.

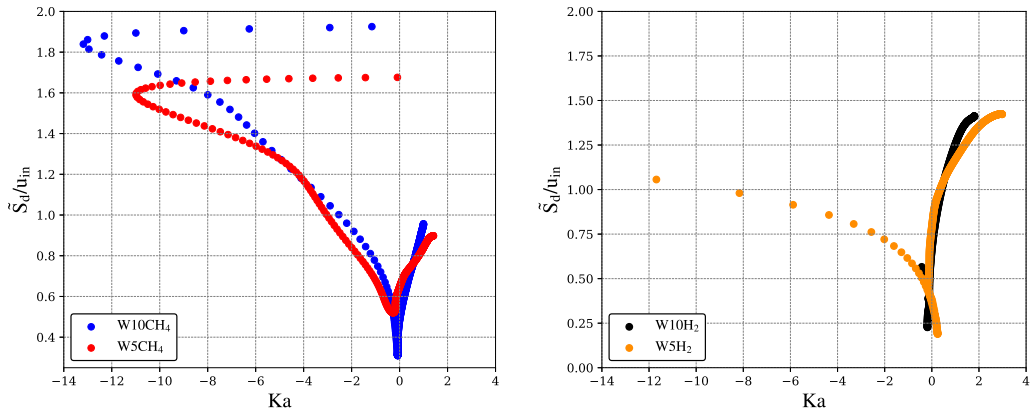


(a) (b)

Figure 6: Correlation between the flame speed and the Ka number for hydrogen and methane cases at $t/\tau_f = 16$ and $t/\tau_f = 32$, respectively, (a) methane and (b) hydrogen cases.

## 5. SUMMARY

Direct numerical simulations were carried out to investigate the effect of the local stretch rate and the mixing layer thickness over the flame speed for hydrogen and methane triple flames. The results show that the triple point is responsible for dominating the entire flame structure for methane flames since that region is associated with higher burning rates. The triple point does not reach the maximum burning speed since it is subjected to positive curvature and the thermo-diffusive effects. The local flame speed and the $\mathrm{Ka}$ correlation show that the curvature and the flame speed mechanism stabilizes the lean flame even in the flammability limit conditions. The hydrogen leading edge is dominated by the richer region where the flame speed becomes faster, and as consequence, the relation $\tilde{S}_d/u_{in}$ reaches values higher than unity. The low equivalence ratio regions result in a flame subject to a high stretched region.

The mixing layer effect causes an impact on the magnitude of flame deformation. For the cases with smaller $\delta_m$, the $\mathrm{Ka}$ number reaches higher values near the leading edge for $\mathrm{H_2}$ and $\mathrm{CH_4}$. The increasing in $\delta_m$ produces a more extended front prevailing values of $\mathrm{Ka_c} \approx 0$ in the intermediate region between $\mathrm{Ka} < 0$ and $\mathrm{Ka} > 0$.

The effects of the front deformation in connection to the flame speed showed that hydrogen and methane triple flames have both a similar response in which the flame speed decreases from $\mathrm{Ka} > 0$ to $Ka \to 0$. It was found that the expected behavior, related to the Markstein length is not required in a partially premixed flame according to the premixed properties.

## 6. ACKNOWLEDGMENTS

The authors gratefully acknowledge the research group of Engler-Bunte-Institute, Division of Combustion Technology, Karlsruhe Institute of Technology, Germany, for providing the EBI-DNS solver, the support of the Scientific Computation Laboratory of Campus Joinville/UFSC, of the Graduate Program in Mechanical Engineering at Federal University of Santa Catarina, Brazil and the National Laboratory for Scientific Computing (LNCC/MCTI, Brazil) for providing HPC resources of the SDumont supercomputer.

## 7. REFERENCES

Benajes, J., García, A., Domenech, V. and Durrett, R., 2013. "An investigation of partially premixed compression ignition combustion using gasoline and spark assistance". *Applied Thermal Engineering*, Vol. 52, No. 2, pp. 468–477.

Buckmaster, J. and Matalon, M., 1989. "Anomalous lewis number effects in tribrachial flames". *Symposium (International) on Combustion*, Vol. 22, No. 1, pp. 1527–1535.

Cadrazco, M., Santamaría, A., Jaramillo, I.C., Kaur, K., Kelly, K. and Agudelo, J.R., 2020. "Characterization of renewable diesel particulate matter gathered from non-premixed and partially premixed flame burners and from a diesel engine". *Combustion and Flame*, Vol. 214, pp. 65–79.

Davis, S., Quinard, J. and Searby, G., 2002. "Markstein numbers in counterflow, methane- and propane- air flames: a computational study". *Combustion and Flame*, Vol. 130, No. 1, pp. 123–136.

Favier, V., Vervisch, L., Herrmann, M., Terhoeven, P., Binninger, B. and Peters, N., 1998. *Numerical Simulation of Combustion in Partially Premixed Turbulent Flows*, Springer Berlin Heidelberg, Berlin, Heidelberg, pp. 203–221.

Ferziger, J.H. and Peric, M., 2002. *Computational Methods for Fluid Dynamics*. Springer, Berlin.

Goodwin, D., 2002. *Cantera C++ user's guide*. California Institute of Technology, California.

Hartley, L.J. and Dold, J.W., 1991. "Flame propagation in a nonuniform mixture: Analysis of a propagating triple-flame". *Combustion Science and Technology*, Vol. 80, No. 1-3, pp. 23–46.

Im, H. and Chen, J., 1999. "Structure and propagation of triple flames in partially premixed hydrogen–air mixtures". *Combustion and Flame*, Vol. 119, No. 4, pp. 436–454.

Im, H.G. and Chen, J.H., 2001. "Effects of flow strain on triple flame propagation". *Combustion and Flame*, Vol. 126, No. 1, pp. 1384–1392.

Ishaq, H., Dincer, I. and Crawford, C., 2022. "A review on hydrogen production and utilization: Challenges and opportunities". *International Journal of Hydrogen Energy*, Vol. 47, No. 62, pp. 26238–26264.

Kee, R., Grcar, J., Smooke, M., Miller, J. and Meeks, E., 1985. "Premix: A fortran program for modeling steady laminar one-dimensional premixed flames". *Sandia National Laboratories*.

Kioni, P., Rogg, B., Bray, K. and Liñán, A., 1993. "Flame spread in laminar mixing layers: The triple flame". *Combustion and Flame*, Vol. 95, No. 3, pp. 276–290.

Lee, B. and Chung, S., 1997. "Stabilization of lifted tribrachial flames in a laminar nonpremixed jet". *Combustion and Flame*, Vol. 109, No. 1, pp. 163–172.

Li, J., Zhao, Z., Kazakov, A. and Dryer, F., 2004. "An updated comprehensive kinetic model of hydrogen combustion". *International Journal of Chemical Kinetics*, Vol. 36, pp. 566 – 575.

Masri, A., 2021. "Challenges for turbulent combustion". *Proceedings of the Combustion Institute*, Vol. 38, No. 1, pp. 121–155. ISSN 1540-7489.

Mosiria, D.B., Huang, R.F. and Hsu, C.M., 2018. "Backward-Inclined Diffusion Jet Flames in Crossflow at Low Jet-to-

Crossflow Momentum Flux Ratios". *Journal of Engineering for Gas Turbines and Power*, Vol. 141, No. 5.

OpenCFD, 2011. "Openfoam user guide". version 2.0.1.

Peters, N. and Williams, F., 1987. "The asymptotic structure of stoichiometric methaneair flames". *Combustion and Flame*, Vol. 68, No. 2, pp. 185–207.

Peters, N., 2001. "Turbulent combustion".

See, Y.C. and Ihme, M., 2015. "Large eddy simulation of a partially-premixed gas turbine model combustor". *Proceedings of the Combustion Institute*, Vol. 35, No. 2, pp. 1225–1234.

van Oijen, J.A. and de Goey, L.P.H., 2004. "A numerical study of confined triple flames using a flamelet-generated manifold". *Combustion Theory and Modelling*, Vol. 8, No. 1, pp. 141–163.

Zirwes, T., Zhang, F., Habisreuther, P., Hansinger, M., Bockhorn, H., Pfitzner, M. and Trimisn, D., 2020. "Quasi-dns dataset of a piloted flame with inhomogeneous inlet conditions". *Flow, Turbulence and Combustion*, Vol. 104, pp. 997–1027.

## 8. RESPONSIBILITY NOTICE

The authors are solely responsible for the printed material included in this paper.